







## PAPER

View Article Online  
View Journal | View Issue

# Uptake of ammonia by ice surfaces at atmospheric temperatures†

Clemens Richter, <sup>\*a</sup> Shirin Gholami,<sup>a</sup> Yanisha Manoharan,<sup>b</sup> Tillmann Buttersack, <sup>a</sup> Luca Longetti, <sup>b</sup> Luca Artiglia, <sup>b</sup> Markus Ammann, <sup>b</sup> Thorsten Bartels-Rausch <sup>\*b</sup> and Hendrik Bluhm <sup>\*a</sup>

Received 14th October 2024, Accepted 11th November 2024

DOI: 10.1039/d4fd00169a

We present an ambient pressure X-ray photoelectron spectroscopy investigation of the adsorption of ammonia on ice over the temperature range  $-23\text{ }^{\circ}\text{C}$  to  $-50\text{ }^{\circ}\text{C}$ . Previous flow tube studies have shown significant uptake of ammonia to ice at these temperatures, which was linked to the incorporation of ammonium into the ice crystal lattice. Our present investigation shows a significant uptake of ammonia to the ice interface, with ammonia concentrations exceeding those measured in past studies for the case of bulk snow and ice. We also have indication that some of the ammonia is protonated at the ice surface and thus adsorbed there as ammonium ions. The impact of high ammonia concentrations at the air–ice interface on the surface chemistry of ice clouds is discussed. The present study lays the groundwork for investigating the reaction of adsorbed ammonia with other trace gases in the atmosphere, which is demonstrated with the example of a proof-of-principle experiment of ammonia's interaction with acetic acid.

## 1 Introduction

Ammonia ( $\text{NH}_3$ ) plays a central role in determining the pH value of atmospheric cloud droplets and aerosol particles.<sup>1–3</sup> It is the most abundant alkaline trace gas in the troposphere<sup>4</sup> with typical atmospheric concentrations in the sub-ppb to tens of ppb range.<sup>5</sup> The interaction of  $\text{NH}_3$  with acidic trace gases is a key mechanism for the nucleation and formation of secondary aerosols in the atmosphere.<sup>6</sup> This reaction leads to the formation of ammonium ( $\text{NH}_4^+$ ) species, a major inorganic aerosol component worldwide.<sup>7</sup> It has also been detected, for instance, in Antarctic coastal snow, after long-range transport and wet

<sup>a</sup>Fritz Haber Institute of the Max Planck Society, Faradayweg 4–6, 14195 Berlin, Germany. E-mail: bluhm@fhi-berlin.mpg.de; crichter@fhi-berlin.mpg.de

<sup>b</sup>PSI Center for Energy and Environmental Sciences, Paul Scherrer Institute, CH-5232 Villigen PSI, Switzerland. E-mail: thorsten.bartels-rausch@psi.ch

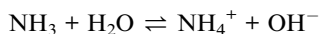
† Electronic supplementary information (ESI) available. See DOI: <https://doi.org/10.1039/d4fd00169a>



precipitation.<sup>8</sup> Abbatt *et al.*<sup>9</sup> and Wentworth *et al.*<sup>10</sup> suggest that the bidirectional NH<sub>3</sub> exchange between the atmosphere and the land–ocean surface is significant and needs to be included in chemical transport models. This is demonstrated by the fact that NH<sub>3</sub> was detected in the Arctic<sup>9</sup> as well as in the upper troposphere,<sup>11</sup> where cirrus clouds are well known to adsorb acidic trace gases and thus impact their atmospheric budget.<sup>12</sup>

Despite its abundance and importance in atmospheric multiphase processes and reactions, the acid–base chemistry of NH<sub>3</sub> in contact with ice and snow under conditions relevant to the Earth's cryosphere has so far not been studied in detail. This is an important gap in our knowledge in view of the rising NH<sub>3</sub> concentrations in the atmosphere, in particular over the last decade. The concentration of NH<sub>3</sub> in the atmosphere is expected to continue to rise due to, *e.g.*, the increased use of nitrogen-containing fertilizers. This development shifts the composition of atmospheric reactive nitrogen from oxidized nitrogen compounds toward a greater prevalence of reduced nitrogen compounds like NH<sub>3</sub>.<sup>13,14</sup>

It is well known that in aqueous environments NH<sub>3</sub> can undergo protonation to form NH<sub>4</sub><sup>+</sup>:



Our experiments address the question of whether NH<sub>3</sub> adsorbs molecularly on the ice at arctic temperatures (−23 to −52 °C) or whether it undergoes protonation to a significant degree.

Some earlier investigations have addressed the adsorption state of NH<sub>3</sub> on ice, albeit at temperatures well below those in the Arctic or the upper parts of the troposphere. The study by Ogasawara *et al.* indicated a rapid protonation of NH<sub>3</sub> when the ice substrate was heated from −235 °C to −153 °C,<sup>15</sup> a result that was also supported by Monte Carlo simulations.<sup>16</sup> A subsequent investigation by Lee and Kang<sup>17</sup> was carried out at higher temperatures (around −70 °C), but did not show any indication for the protonation of NH<sub>3</sub>, which would have been expected if protonation is observed already at lower temperatures. Lee and Kang argued that the protonation observed in the previous investigation was driven by incomplete wetting of the ice film on the metal substrate and protonation of NH<sub>3</sub> was governed by the interaction with the metal substrate in the presence of water molecules that foster proton transfer. They also showed that at temperatures of around −70 °C incorporation of NH<sub>3</sub> into the ice bulk was negligible.

One major pathway for the trapping of atmospheric trace gases is their incorporation into the bulk of growing ice particles in clouds. Hoog *et al.*<sup>18</sup> argued that ammonia is efficiently trapped by growing ice due to the high solubility of NH<sub>4</sub><sup>+</sup> in water. Indeed, NH<sub>4</sub><sup>+</sup> and NH<sub>3</sub> are generally thought to have a high solubility in ice (about 2 g l<sup>−1</sup>) due to the ability of NH<sub>4</sub><sup>+</sup> to substitute for water molecules in the ice lattice.<sup>19</sup> However, it was pointed out that these measurements are difficult and prone to large uncertainties.<sup>19–21</sup> Kärcher *et al.* proposed that trapping of trace gases in ice is governed by their adsorption at the ice surface and subsequent diffusion into the bulk, a process that is also influenced by the growth rate of the ice crystal.<sup>22,23</sup> Incorporation into bulk ice thus provides a pathway for the uptake of very high amounts of trace gases, compared to trapping mechanisms based on purely surface adsorption. For the case of



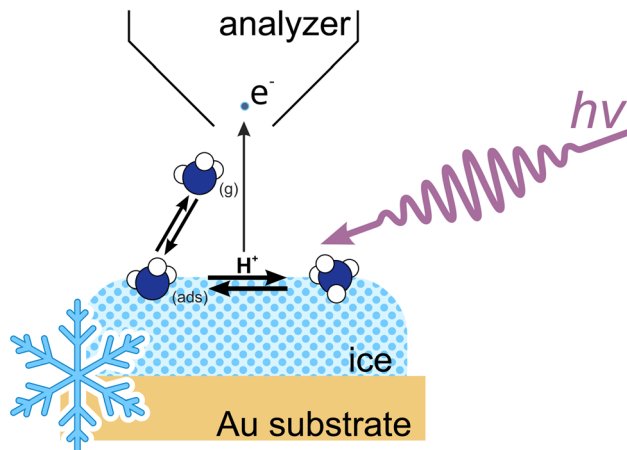


Fig. 1 Schematic of  $\text{NH}_3$  adsorption at the ice–vapor interface in our experimental setup.

ammonia this was shown by Hoog and coworkers<sup>18</sup> who studied the uptake of  $\text{NH}_3$  to ice crystals at temperatures above  $-20^\circ\text{C}$  and  $\text{NH}_3$  gas phase concentrations of up to 10 ppm and found that  $\text{NH}_3$  enters the ice phase as  $\text{NH}_4^+$ , which is then incorporated into the ice lattice.

In addition to the bulk, the interface layer (the first few nanometers) on ice also has a potentially high capacity to capture trace gases, as seen for strong acids such as  $\text{HCl}$  and  $\text{HNO}_3$ .<sup>24,25</sup> To observe this phenomenon, interface-sensitive techniques are required to directly determine the concentration of adsorbed species and to evaluate the impact of surface processes on the trapping of trace gases at the ice–air interface. Our present study thus focuses on the adsorption of ammonia on ice, which we investigate with ambient pressure X-ray photoelectron spectroscopy (APXPS) at temperatures relevant to polar regions and the upper parts of the troposphere (see Fig. 1).

We find evidence that under these conditions  $\text{NH}_3$  is present at the air–ice interface. We also present a proof-of-principle investigation of the heterogeneous reaction of adsorbed  $\text{NH}_3/\text{NH}_4^+$  with a relevant trace gas in the atmosphere – acetic acid. The feasibility of APXPS studies of these phenomena paves the way for in-depth investigations of heterogeneous reactions (*e.g.* the chemical nature of adsorbates and reaction products) on ice surfaces taking place in polar regions and on frozen aqueous aerosol particles occurring in the troposphere.

## 2 Experimental

The experiments were performed at the X07DB *in situ* spectroscopy beamline of the Swiss Light Source (SLS) of the Paul Scherrer Institute using the Ambient Pressure Photoemission endstation.<sup>26</sup> The endstation consists of a differentially pumped hemispherical electron analyzer (Scienta R4000 HiPP-2) attached to a reactor cell with a temperature controlled sample holder. Connected to the reactor cell is a gas dosing system which controls the partial pressures of the trace gases and water vapor. All measurements were performed at partial



pressures of water up to 2.5 mbar to maintain the prepared ice samples in equilibrium with their respective vapor pressure corresponding to the ice temperature. Photon energies were chosen to ensure that spectra from all relevant core-levels were obtained at similar photoelectron kinetic energies of about 245 eV.

## 2.1 Sample preparation

Ice samples were grown on a Au-coated sample holder positioned in the reactor cell at a distance of several millimeters from the differentially-pumped entrance aperture of the electron analyzer. In this position any influence of the reduced water vapor pressure right in front of the aperture is avoided during ice growth. Water vapor was dosed into the reactor cell at a partial pressure slightly exceeding that of the equilibrium vapor pressure at the desired ice temperature to establish a slight oversaturation. Subsequently, the temperature of the sample holder was reduced until the formation of ice nuclei was observed by eye. The formation of ice was also indicated by a decrease of the water vapor pressure in the reactor cell. Once ice nucleation was established the ice was allowed to grow slowly for about 1 hour, until a closed polycrystalline ice film of a few hundred micrometer thickness was formed.

XPS measurements on these ice films were typically performed in an additional flow of Ar in the experimental cell at partial pressures of about 0.2 mbar to 0.4 mbar. This background gas helped to minimize perturbations of the ice due to radiative heating from the reactor cell walls and the aperture of the electron analyzer.<sup>27</sup> In addition, the use of a background gas partially compensates the charging of the insulating ice film due to electron emission and offers the possibility to vary the gas phase composition in the experimental cell at a constant total pressure ( $p_{\text{cell}} = \text{constant}$  on the order of 0.4 to 2.5 mbar).  $\text{NH}_3(\text{g})$  was dosed onto the ice films from a premixed gas mixture of 3%  $\text{NH}_3$  in He. In that manner we were able to dose  $\text{NH}_3$  at partial pressures between  $1.2 \times 10^{-3}$  mbar to  $6.0 \times 10^{-3}$  mbar (1.2 to 6 ppm).

## 2.2 Phototelectron spectroscopy

For each experimental run a set of X-ray photoemission spectra was first taken of the as-prepared ice film at the temperature of interest, and then during the exposure of the ice surface to  $\text{NH}_3$ . We also followed the evolution of the surface chemical composition once the  $\text{NH}_3$  flow into the reactor cell was stopped. Typical durations for a single experiment varied from 2 to more than 5 hours. O 1s and N 1s spectra were taken at photon energies of 780 eV and 650 eV, respectively, to ensure that the photoelectrons from the different core levels have a comparable kinetic energy and thus comparable electron probing depths, which is about 1.7 nm for electrons with a kinetic energy of 250 eV detected at an angle of  $30^\circ$  relative to the surface normal.<sup>28</sup>

The spectra were fitted using the KolXPD software package (Kolibri.net, Czech Republic). For all spectra a linear background was subtracted, and Gaussian peaks were used to fit components due to substrate and adsorbate species. Peaks due to gas phase species were fitted using Voigt profiles. Example spectra and a more detailed description of the fitting routine and constraints are shown in the ESI (see Fig. S4–S7).†



### 3 Results and discussion

In the following, we describe the results of the XPS experiments on the uptake of  $\text{NH}_3$  by ice surfaces. We start with the description of the principal components of the N 1s spectra of as-grown and ammonia-covered ice surfaces before describing the uptake experiments.

#### 3.1 Principal components of the N 1s spectra

Fig. 2(a) shows a representative N 1s spectrum of a freshly prepared ice sample (bottom trace), and that for  $\text{NH}_3$  adsorbed on the same ice sample during exposure to  $\text{NH}_{3(\text{g})}$  when a steady-state of surface adsorption at an ice temperature of  $-35^\circ\text{C}$  was reached (top trace). The freshly-grown ice sample already shows a significant contribution of a nitrogen species (grey-shaded peak), which is due to adventitious contamination, which was present in all prepared ice samples. The precise nature of this species and its origin could not be unambiguously determined, though it is likely due to residual contamination of the reactor cell, which, despite our best efforts, could not be removed. As we will show in the following, this species has only a marginal effect on the results of the investigation since it behaves like a bystander in the uptake experiments. The electron binding energy (BE) of this species is  $402.2(2)\text{ eV}$ , referenced with the literature value of the O 1s BE of polycrystalline ice at  $533.8\text{ eV}$ .<sup>29</sup> Nitrogen species with a similar BE were previously observed in APXPS experiments of  $\text{NO}_2$  adsorbed on  $\text{TiO}_2$  and ascribed to reduced nitrogen.<sup>30</sup> We refer to this nitrogen species in the following as  $\text{N}_{\text{adv}}$ . This  $\text{N}_{\text{adv}}$  signature was invariant over an extended period indicating that it is not accumulating or subject to beam-induced effects (see ESI Fig. S2† for details).

The N 1s spectrum after adsorption of  $\text{NH}_3$  on the same ice substrate is shown in the upper trace of Fig. 2(a). It shows a significantly increased total intensity,

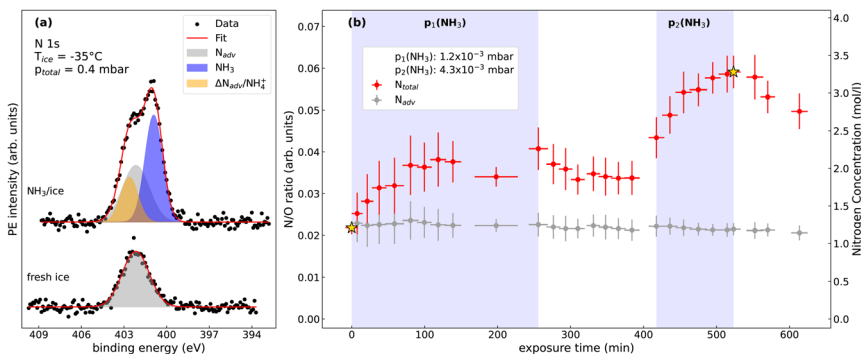


Fig. 2 (a) N 1s spectra of freshly prepared ice (bottom) and  $\text{NH}_3/\text{ice}$  (top) at  $-35^\circ\text{C}$  at a partial pressure  $p(\text{NH}_3)$  of  $4.3 \times 10^{-3}\text{ mbar}$ . The spectra were scaled to the same background intensity. Subsequently, the linear background was subtracted. (b) N/O ratio and estimated concentrations of  $\text{N}_{\text{total}}$  (red) and  $\text{N}_{\text{adv}}$  (grey) as a function of exposure time. Star symbols indicate the data corresponding to spectra shown in (a). Uncertainties on the x-axis stem from the acquisition times required for a set of N 1s and O 1s spectra. Uncertainties in the y-direction have been evaluated as the standard deviation ( $1\sigma$ ) from the signal-to-noise ratios of the core-level spectra.



with the strongest peak at the low BE side. Since this peak increases with increasing exposure to  $\text{NH}_{3(\text{g})}$ , we assign it to  $\text{NH}_3$  adsorbed on ice (blue shaded peak in Fig. 2(a)). The binding energy of adsorbed  $\text{NH}_3$ , referenced to that of the O 1s peak of solid ice, is 400.7(2) eV, a value similar to that for  $\text{NH}_3$  adsorbed on silicon and silicate surfaces.<sup>31,32</sup> The expected position of the gas-phase  $\text{NH}_{3(\text{g})}$  peak, based on literature values (405.5(2) eV)<sup>33</sup> that are referenced to a BE of water vapor (539.8(2) eV),<sup>34</sup> is around 400 eV on the binding energy scale used in this study and depends on the degree of charging of the ice. The N 1s peak due to  $\text{NH}_{3(\text{g})}$  thus overlaps with the signals of the adsorbates. However, due to the low partial pressure of  $\text{NH}_{3(\text{g})}$  in the reactor cell the intensity of this peak is negligible within the signal-to-noise ratio in our experiments.

The additional signal at the high BE side of the spectrum (orange shaded peak) is more difficult to assign due to its overlap with the  $\text{N}_{\text{adv}}$  signature. This species could reasonably be interpreted as a time-dependent increase in the  $\text{N}_{\text{adv}}$  intensity, or that it is due to a new nitrogen species, for instance  $\text{NH}_4^+$  which is formed by the protonation of adsorbed  $\text{NH}_3$ . The latter would be consistent with observations in previous experiments.<sup>15</sup>

Since we cannot unambiguously assign this feature to  $\text{NH}_4^+$ , we label it for the moment as  $\Delta\text{N}_{\text{adv},\text{NH}_4^+}$ . The  $\Delta\text{N}_{\text{adv},\text{NH}_4^+}$  peak has a binding energy of 402.5(2) eV, *i.e.* 1.8(2) eV higher than the BE of  $\text{NH}_3$ , which is in good agreement with the value for  $\text{NH}_4^+$  in aqueous solution.<sup>35,36</sup> The higher binding energy of  $\text{NH}_4^+$  compared to  $\text{NH}_3$  can be related to its positive charge. The sensitivity of XPS to the charge state has been used previously to discuss the protonation of acids at the solution–vapor<sup>37</sup> and air–ice interface.<sup>38–41</sup>

### 3.2 Adsorption of $\text{NH}_3$

We now turn our attention to the evolution of the N 1s spectra during the exposure of ice to  $\text{NH}_{3(\text{g})}$  as a function of time and partial pressure. To follow and quantify the uptake of  $\text{NH}_3$  by ice, alternating N 1s and O 1s core level spectra were recorded using photon energies of 650 eV and 780 eV, respectively, to ensure a comparable probing depth, as described above. The N 1s spectra provide information on the chemical nature of the adsorbed  $\text{NH}_3$  species, while O 1s spectra serve as a reference to quantify the adsorbate concentration and to monitor potential charging effects due to the photoemission process.

Fig. 2(b) shows the experimentally-determined atomic N/O ratio for the ice film at  $-35^\circ\text{C}$  as a function of exposure time at two different nominal  $\text{NH}_{3(\text{g})}$  partial pressures of  $p_1 = 1.2 \times 10^{-3}$  mbar and  $p_2 = 4.3 \times 10^{-3}$  mbar. The N 1s and O 1s intensities were normalized to the respective photoionization cross sections,<sup>42</sup> and the photon flux. As the photoelectron intensity is directly proportional to the amount of the species of interest in the probed volume, the normalized N/O ratio serves as a measure of the concentration of adsorbed nitrogen species on ice. These data do not reveal the precise distribution of the adsorbates within the probed volume at the interface, *i.e.* whether they are just adsorbed to the surface or evenly distributed across the probed volume. For simplicity we present in Fig. 2(b) the volumetric concentrations assuming an even distribution of nitrogen species in the near-surface region.

The estimated volumetric nitrogen concentrations are shown on the right axis in Fig. 2(b), assuming one N atom per molecule. The red symbols represent the N/



O ratio for the total nitrogen intensity, here referred to as  $N_{\text{total}}$ , grey symbols show the N/O ratio of the reduced nitrogen  $N_{\text{adv}}$  determined from the deconvoluted N 1s spectra. Shaded background areas indicate the time intervals in which  $\text{NH}_{3(\text{g})}$  was dosed onto the ice film. The N 1s spectrum for the freshly prepared ice film in the absence of  $\text{NH}_{3(\text{g})}$  in the reactor cell is shown in Fig. 2(a), bottom trace, and was already discussed in the previous section. Upon adjusting the partial pressure to  $p(\text{NH}_{3(\text{g})}) = 1.2 \times 10^{-3}$  mbar, the N/O ratio starts to increase. Over a time of around 100 min a rise in the N/O ratio is observed, with the N/O ratio roughly doubling over this time period. After about 100 min the N/O ratio reaches a plateau, indicating a steady state of  $\text{NH}_3$  adsorption/desorption.

When the flow of  $\text{NH}_{3(\text{g})}$  into the reactor cell is stopped after about 250 min (see Fig. 2(b)), only a slight decrease in the N/O ratio is observed, most likely due to the slow pump-out of  $\text{NH}_{3(\text{g})}$  from the reactor cell driven by retention and release from the reactor walls. Subsequently, at about 410 min the  $\text{NH}_{3(\text{g})}$  partial pressure was increased to a higher value of  $p(\text{NH}_{3(\text{g})}) = 4.3 \times 10^{-3}$  mbar, again resulting in a nonlinear increase in  $N_{\text{total}}$ , eventually leading to a tripling of the original N/O ratio at about 500 min. The  $\text{NH}_{3(\text{g})}$  flow was then stopped again, upon which a noticeable decrease of the N/O ratio is observed, indicating desorption of N species from the ice surface. A subset of the XPS spectra from which the N/O ratios in Fig. 2(b) are extracted is shown in the ESI.†

The fit of the N 1s data using constraints derived from the fit of the as-grown ice sample (Fig. 2(a)) shows that the peak area and thus the surface concentration of the adventitious N contamination ( $N_{\text{adv}}$ ), represented by the grey symbols in Fig. 2(b)), was constant during the whole time of the adsorption/desorption experiment. The increase in the  $N_{\text{total}}$  signal as a function of the exposure time is governed by the adsorption of  $\text{NH}_3$ , which also shows reversibility under desorption conditions.

For a detailed look at the  $\text{NH}_3$  adsorption we plot the N/O ratios of the deconvoluted N 1s peak areas of  $\text{NH}_3$  (blue) and  $\Delta N_{\text{adv},\text{NH}_4^+}$  (orange) as a function of exposure time for the  $-35^\circ\text{C}$  ice sample in Fig. 3. The adventitious nitrogen contamination is not included in this graph.  $\text{NH}_3$  is the main adsorbed species and thus shows the same behavior with time and exposure as  $N_{\text{total}}$  in Fig. 2(b), *i.e.*, it displays an increase during  $\text{NH}_{3(\text{g})}$  dosage and a noticeable decrease when the  $\text{NH}_{3(\text{g})}$  flow into the reactor cell is stopped.

The  $\Delta N_{\text{adv},\text{NH}_4^+}$  species (see Fig. 3) shows a slightly different behavior compared to  $\text{NH}_3$  during  $\text{NH}_{3(\text{g})}$  dosing, in particular a delayed appearance and slower increase in its abundance. This is observed for both  $\text{NH}_{3(\text{g})}$  dosing steps, and also for the decrease in abundance when the  $\text{NH}_{3(\text{g})}$  flow into the reactor cell is stopped. In particular in the case of desorption following the uptake of  $\text{NH}_{3(\text{g})}$  at the higher partial pressure (*i.e.*, after 520 min in Fig. 3) the decrease in intensity of the  $\Delta N_{\text{adv},\text{NH}_4^+}$  peak does not follow that of the peak due to adsorbed  $\text{NH}_3$ . Possible explanations for this behavior are: (i) that a fraction of the adsorbed  $\text{NH}_3$  undergoes protonation to  $\text{NH}_4^+$ , which has slower desorption kinetics; and (ii) that the amount of adventitious nitrogen ( $N_{\text{adv}}$ ) increases over time during the exposure to  $\text{NH}_{3(\text{g})}$ , possibly also due to photochemical reactions induced by the incident X-rays. While it is likely that  $\text{NH}_3$  engages in acid–base chemistry to form  $\text{NH}_4^+$  as was observed in other studies,<sup>15,18,43</sup> a change in  $N_{\text{adv}}$  cannot be completely ruled out due to the strong overlap in binding energy of the  $\text{NH}_4^+$  and  $N_{\text{adv}}$  species.





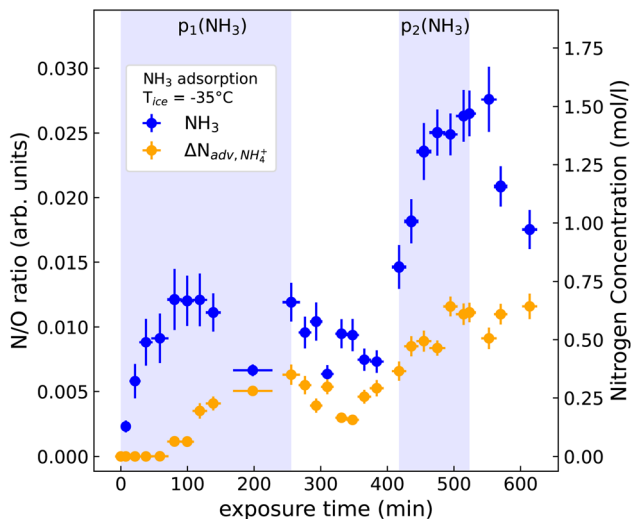


Fig. 3 N/O ratio and estimated concentrations of  $\text{NH}_3$  (blue) and  $\Delta\text{N}_{\text{adv},\text{NH}_4^+}$  (orange) as a function of exposure time. Uncertainties on the x-axis stem from the acquisition times required for a set of N 1s and O 1s spectra. Uncertainties in the y-direction have been evaluated as the standard deviation ( $1\sigma$ ) from the signal-to-noise ratios of the core-level spectra.

### 3.3 Estimate of the $\text{NH}_3$ concentration

The data presented above were obtained for an ice film at  $-35^\circ\text{C}$ . In addition, we have performed measurements at a number of other temperatures ranging from  $-23^\circ\text{C}$  to  $-52^\circ\text{C}$ , with each measurement starting with the preparation of a fresh ice sample. From the measured N/O ratios the concentrations of  $\text{N}_{\text{total}}$ ,  $\text{N}_{\text{adv}}$ ,  $\text{NH}_3$  and  $\Delta\text{N}_{\text{adv},\text{NH}_4^+}$  are determined and compiled in Table 1. The data show that  $C_{\text{N}_{\text{adv}}}$  increases with decreasing ice temperature. We note that the partial pressures of

Table 1 Compilation of concentrations of nitrogen species on ice film between  $-23^\circ\text{C}$  and  $-52^\circ\text{C}$ . The concentrations have been determined from experimentally determined N/O ratios using XPS.  $T_{\text{ice}}$  is given in  $^\circ\text{C}$ ,  $p(\text{NH}_3)$  in mbar and concentrations are given in  $\text{mol l}^{-1}$ . Asterisks (\*) indicate ice samples prepared in a separate experimental campaign in which  $\text{N}_{\text{adv}}$  was significantly higher

$T_{\text{ice}}$	$p(\text{NH}_3)$	$C_{\text{N}_{\text{total}}}$	$C_{\text{N}_{\text{adv}}}$	$C_{\text{NH}_3}$	$C(\Delta\text{N}_{\text{adv},\text{NH}_4^+})$
$-23$	0.0043	1.9(3)	0.9(1)	0.5(1)	0.5(1)
$-23$	0.006	2.9(4)	0.9(1)	1.2(2)	0.8(1)
$-29^*$	0.0012	7.3(1.0)	4.5(6)	1.8(3)	1.0(1)
$-35$	0.0012	2.1(2)	1.3(1)	0.5(1)	0.3(1)
$-35$	0.0043	3.3(3)	1.2(1)	1.5(1)	0.6(1)
$-45^*$	0.0012	7.1(1.3)	5.5(1.0)	1.6(3)	0.0(1)
$-45$	0.0024	3.6(6)	2.1(3)	1.0(2)	0.5(1)
$-45$	0.006	4.4(6)	2.2(3)	1.7(2)	0.5(1)
$-52$	0.0012	5.8(1.1)	3.9(7)	0.7(1)	1.2(2)
$-52$	0.0024	5.3(7)	3.1(4)	1.3(2)	1.0(1)
$-52$	0.006	6.4(8)	3.1(4)	2.3(3)	0.9(1)



NH<sub>3</sub>, listed in Table 1, are upper estimates based on the concentration of gas entering the experimental set-up. Potential wall losses are not accounted for.

The clear separation of the NH<sub>3</sub> species in the XPS spectra (Fig. 2(a)) allows us to discuss its concentration within our probing depth in more detail and set them in the context of literature values for the uptake of NH<sub>3</sub> by ice and snow. The values for NH<sub>3</sub> concentration from our measurements in Table 1 are of the order of 0.5 to 2.3 mol l<sup>-1</sup> (*i.e.*, about 8 to 34 g l<sup>-1</sup>). These values are higher than the upper concentrations for ammonia or ammonium in bulk ice (up to 0.01 mol l<sup>-1</sup> for NH<sub>4</sub><sup>+</sup>).<sup>19,44,45</sup> They are also higher than those found by Hoog and coworkers<sup>18</sup> for ammonium trapped in bulk ice at -20 °C, which are <0.1 mg l<sup>-1</sup> for similar gas-phase concentrations as in our experiments.

The higher concentration of NH<sub>3(ads)</sub> in our experiments compared to the literature values obtain from volumetric measurements, indicates that NH<sub>3</sub> is enriched in the surface region, since XPS exclusively probes the narrow interfacial region of the ice samples. If one assumes that all of the NH<sub>3</sub> within our probing depth of about 1.7 nm is concentrated in a single layer at the very surface between the ice and vapor phase, the 2D concentration of NH<sub>3</sub> would be about 3 × 10<sup>14</sup> molecules per cm<sup>2</sup>, *i.e.* about one third of the concentration of water molecules in the surface layer. As we have already pointed out, we do not have information on the distribution of NH<sub>3</sub> in the near surface layer, or the potential influence of the liquid-like layer, so the estimates for a pure surface layer (3 × 10<sup>14</sup> molecules per cm<sup>2</sup>) and NH<sub>3</sub> evenly distributed throughout the near-surface region (up to 2.3 mol l<sup>-1</sup>), are limiting cases for possible adsorption behavior scenarios. Either model shows, however, that the interfacial layer can hold even higher amounts of ammonium than the total amounts in the bulk of ice crystals. The fate of this interfacially trapped ammonium and ammonia over time needs further study to evaluate its impact on cloud scavenging.

## 4 Conclusions and outlook

In this article we showed that ambient pressure X-ray photoelectron spectroscopy is an excellent method to follow the uptake of ammonia on ice surfaces at atmospherically-relevant temperatures. We showed that APXPS is able to quantify the amount of adsorbed ammonia and to determine the chemical nature of the adsorbed species *via* the characteristic N 1s electron binding energy. The data demonstrate that ammonia adsorbs mainly in its neutral form (NH<sub>3</sub>), with some of the molecules most likely undergoing protonation to NH<sub>4</sub><sup>+</sup>.

We were able to make these observation even in the presence of adventitious nitrogen contamination. This kind of contamination is a serious issue in any measurement under atmospherically-relevant conditions, *i.e.* far away from ultra-high vacuum conditions and at appreciable partial pressures of water vapor without large pumping speeds. This underlines the need for dedicated and easily cleanable reactor cells for studies of ice surfaces in the presence of reactive trace gases.

The present study builds on past experiments on the investigation of trace gas uptake by ice surfaces using APXPS.<sup>29,38,46,47</sup> The success of these measurements opens up opportunities to not only study the adsorption of a single trace gas species, but also to investigate the co-adsorption and possible reactions of



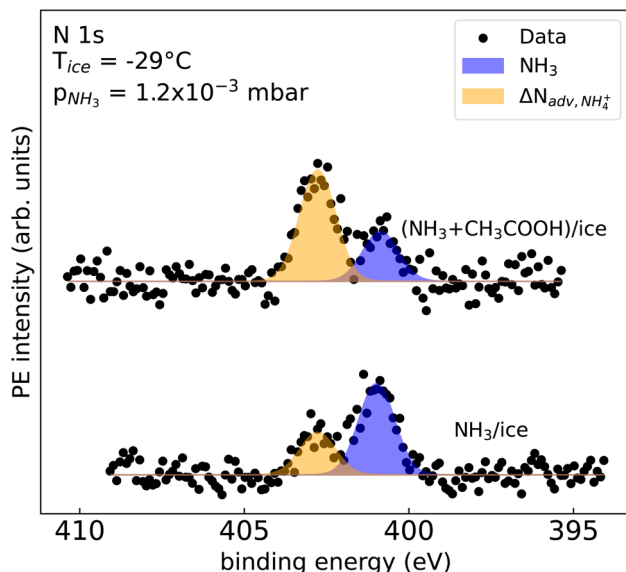


Fig. 4 N 1s spectra of  $\text{NH}_3/\text{ice}$  at  $-29^\circ\text{C}$  at a partial pressure  $p(\text{NH}_3)$  of  $1.2 \times 10^{-3}$  mbar with (top) and without (bottom) acetic acid as the co-adsorbent. The spectra were scaled to the same background intensity. The linear background and the  $\text{N}_{\text{adv}}$  signal contribution was subtracted. The unsubtracted spectra are shown in the ESI.†

multiple trace gas species, with the ice surface potentially acting as a catalyst for a heterogeneous reaction between the adsorbates.

We therefore conclude this paper with the result of a proof-of-principle study of the co-adsorption of  $\text{NH}_3$  with acetic acid ( $\text{CH}_3\text{COOH}$ ). The N 1s spectra that compare the adsorption of  $\text{NH}_3$  with the case for  $\text{CH}_3\text{COOH}/\text{NH}_3$  co-adsorption are shown in Fig. 4. The bottom trace shows the initially prepared  $\text{NH}_3/\text{ice}$  surface at  $p(\text{NH}_3) = 1.2 \times 10^{-3}$  mbar. The top trace shows the same ice film after dosing  $\text{NH}_3$  and  $\text{CH}_3\text{COOH}$  simultaneously. While the signal contribution of  $\text{NH}_3$  (blue) is more pronounced compared to  $\Delta\text{N}_{\text{adv},\text{NH}_4^+}$  (orange) on  $\text{NH}_3/\text{ice}$ , the  $\Delta\text{N}_{\text{adv},\text{NH}_4^+}$  intensity significantly increases in the presence of  $\text{CH}_3\text{COOH}$ . In addition a decrease in the  $\text{NH}_3$  intensity was observed. This indicates an interaction of  $\text{NH}_3$  and  $\text{CH}_3\text{COOH}$  at the ice–vapor interface, likely leading to the formation of ammonium acetate.

We believe that this initial result holds promise for future investigations of more complex reactions at ice surfaces in the presence of a mix of trace gas species at their atmospheric concentrations and relevant ice temperatures. The strength of APXPS studies is that they are able to monitor the chemical nature of the adsorbate, *e.g.* its protonation state, and provide complementary information to flow tube studies, which are sensitive to the gas phase composition of reactants and products.

## Data availability

Data for this article, including the data displayed in Fig. 2–4 will be made available at our Zenodo repository “Uptake of Ammonia by Ice Surfaces at Atmospheric Temperatures” upon acceptance of the manuscript.



## Author contributions

CR conceived the project and analyzed the experimental data. CR, TBR and HB wrote the manuscript with critical feedback from all co-authors. CR, SG, YM, TB, LL, TBR and HB performed measurements. LA provided the endstation and support for the spectroscopic measurements. HB, MA and TBR supervised the project.

## Conflicts of interest

There are no conflicts to declare.

## Acknowledgements

We acknowledge funding from the Swiss National Science Foundation, Switzerland (Grant 178 962). The technical support from Andrés Laso is highly appreciated. We thank the staff of the PSI/SLS for excellent beam quality and the beamline scientists at ISS for their support. SG acknowledges support by the International Max Planck Research School on Elementary Processes in Physical Chemistry, Berlin, Germany. Open Access funding provided by the Max Planck Society.

## References

- 1 A. Nenes, S. N. Pandis, R. J. Weber and A. Russell, *Atmos. Chem. Phys.*, 2020, **20**, 3249–3258.
- 2 A. Tilgner, T. Schaefer, B. Alexander, M. Barth, J. L. Collett Jr, K. M. Fahey, A. Nenes, H. O. T. Pye, H. Herrmann and V. F. McNeill, *Atmos. Chem. Phys.*, 2021, **21**, 13483–13536.
- 3 G. Zheng, H. Su and Y. Cheng, *Environ. Sci. Technol.*, 2023, **57**, 12571–12582.
- 4 S. N. Behera, M. Sharma, V. P. Aneja and R. Balasubramanian, *Environ. Sci. Pollut. Res.*, 2013, **20**, 8092–8131.
- 5 Y. You, V. P. Kanawade, J. A. de Gouw, A. B. Guenther, S. Madronich, M. R. Sierra-Hernández, M. Lawler, J. N. Smith, S. Takahama, G. Ruggeri, A. Koss, K. Olson, K. Baumann, R. J. Weber, A. Nenes, H. Guo, E. S. Edgerton, L. Porcelli, W. H. Brune, A. H. Goldstein and S.-H. Lee, *Atmos. Chem. Phys.*, 2014, **14**, 12181–12194.
- 6 M. Wang, M. Xiao, B. Bertozzi, G. Marie, B. Rörup, B. Schulze, R. Bardakov, X.-C. He, J. Shen, W. Scholz, R. Marten, L. Dada, R. Baalbaki, B. Lopez, H. Lamkaddam, H. E. Manninen, A. Amorim, F. Ataei, P. Bogert, Z. Brasseur, L. Caudillo, L.-P. De Menezes, J. Duplissy, A. M. L. Ekman, H. Finkenzeller, L. G. Carracedo, M. Granzin, R. Guida, M. Heinritzi, V. Hofbauer, K. Höhler, K. Korhonen, J. E. Krechmer, A. Kürten, K. Lehtipalo, N. G. A. Mahfouz, V. Makhmutov, D. Massabò, S. Mathot, R. L. Mauldin, B. Mentler, T. Müller, A. Onnela, T. Petäjä, M. Philippov, A. A. Piedehierro, A. Pozzer, A. Ranjithkumar, M. Schervish, S. Schobesberger, M. Simon, Y. Stozhkov, A. Tomé, N. S. Umo, F. Vogel, R. Wagner, D. S. Wang, S. K. Weber, A. Welti, Y. Wu, M. Zauner-Wieczorek, M. Sipilä, P. M. Winkler, A. Hansel, U. Baltensperger, M. Kulmala,



- R. C. Flagan, J. Curtius, I. Riipinen, H. Gordon, J. Lelieveld, I. El-Haddad, R. Volkamer, D. R. Worsnop, T. Christoudias, J. Kirkby, O. Möhler and N. M. Donahue, *Nature*, 2022, **605**, 483–489.
- 7 J. L. Jimenez, M. R. Canagaratna, N. M. Donahue, A. S. H. Prevot, Q. Zhang, J. H. Kroll, P. F. DeCarlo, J. D. Allan, H. Coe, N. L. Ng, A. C. Aiken, K. S. Docherty, I. M. Ulbrich, A. P. Grieshop, A. L. Robinson, J. Duplissy, J. D. Smith, K. R. Wilson, V. A. Lanz, C. Hueglin, Y. L. Sun, J. Tian, A. Laaksonen, T. Raatikainen, J. Rautiainen, P. Vaattovaara, M. Ehn, M. Kulmala, J. M. Tomlinson, D. R. Collins, M. J. Cubison, J. Dunlea, J. A. Huffman, T. B. Onasch, M. R. Alfarra, P. I. Williams, K. Bower, Y. Kondo, J. Schneider, F. Drewnick, S. Borrmann, S. Weimer, K. Demerjian, D. Salcedo, L. Cottrell, R. Griffin, A. Takami, T. Miyoshi, S. Hatakeyama, A. Shimono, J. Y. Sun, Y. M. Zhang, K. Dzepina, J. R. Kimmel, D. Sueper, J. T. Jayne, S. C. Herndon, A. M. Trimborn, L. R. Williams, E. C. Wood, A. M. Middlebrook, C. E. Kolb, U. Baltensperger and D. R. Worsnop, *Science*, 2009, **326**, 1525–1529.
- 8 M. Legrand, F. Ducroz, D. Wagenbach, R. Mulvaney and J. Hall, *J. Geophys. Res.*, 1998, **103**, 11043–11056.
- 9 J. P. D. Abbatt, W. R. Leaitch, A. A. Aliabadi, A. K. Bertram, J.-P. Blanchet, A. Boivin-Rioux, H. Bozem, J. Burkart, R. Y. W. Chang, J. Charette, J. P. Chaubey, R. J. Christensen, A. Cirisan, D. B. Collins, B. Croft, J. Dionne, G. J. Evans, C. G. Fletcher, M. Galí, R. Ghahreman, E. Girard, W. Gong, M. Gosselin, M. Gourdal, S. J. Hanna, H. Hayashida, A. B. Herber, S. Hesaraki, P. Hoor, L. Huang, R. Hussherr, V. E. Irish, S. A. Keita, J. K. Kodros, F. Köllner, F. Kolonjari, D. Kunkel, L. A. Ladino, K. Law, M. Levasseur, Q. Libois, J. Liggio, M. Lizotte, K. M. Macdonald, R. Mahmood, R. V. Martin, R. H. Mason, L. A. Miller, A. Moravek, E. Mortenson, E. L. Mungall, J. G. Murphy, M. Namazi, A.-L. Norman, N. T. O'Neill, J. R. Pierce, L. M. Russell, J. Schneider, H. Schulz, S. Sharma, M. Si, R. M. Staebler, N. S. Steiner, J. L. Thomas, K. von Salzen, J. J. B. Wentzell, M. D. Willis, G. R. Wentworth, J.-W. Xu and J. D. Yakobi-Hancock, *Atmos. Chem. Phys.*, 2019, **19**, 2527–2560.
- 10 G. R. Wentworth, J. G. Murphy, B. Croft, R. V. Martin, J. R. Pierce, J.-S. Côté, I. Courchesne, J.-E. Tremblay, J. Gagnon, J. L. Thomas, S. Sharma, D. Toom-Sauntry, A. Chivulescu, M. Levasseur and J. P. D. Abbatt, *Atmos. Chem. Phys.*, 2016, **16**, 1937–1953.
- 11 M. Höpfner, R. Volkamer, U. Grabowski, M. Grutter, J. Orphal, G. Stiller, T. von Clarmann and G. Wetzel, *Atmos. Chem. Phys.*, 2016, **16**, 14357–14369.
- 12 P. J. Popp, T. P. Marcy, L. A. Watts, R. S. Gao, D. W. Fahey, E. M. Weinstock, J. B. Smith, R. L. Herman, R. F. Troy, C. R. Webster, L. E. Christensen, D. G. Baumgardner, C. Voigt, B. Kärcher, J. C. Wilson, M. J. Mahoney, E. J. Jensen and T. P. Bui, *Geophys. Res. Lett.*, 2007, **34**, L24812.
- 13 R. W. Pinder, K. W. Appel and R. L. Dennis, *Environ. Pollut.*, 2011, **159**, 3138–3141.
- 14 S. J. Pai, C. L. Heald and J. G. Murphy, *ACS Earth Space Chem.*, 2021, **5**, 1674–1685.
- 15 H. Ogasawara, N. Horimoto and M. Kawai, *J. Chem. Phys.*, 2000, **112**, 8229–8232.
- 16 N. Uras, V. Buch and J. P. Devlin, *J. Phys. Chem. B*, 2000, **104**, 9203–9209.



- 17 D. H. Lee and H. Kang, *J. Phys. Chem. C*, 2023, **127**, 2885–2893.
- 18 I. Hoog, S. K. Mitra, K. Diehl and S. Borrmann, *J. Atmos. Chem.*, 2007, **57**, 73–84.
- 19 P. V. Hobbs, *Ice Physics*, OUP Oxford, 2010.
- 20 T. Huthwelker, M. Ammann and T. Peter, *Chem. Rev.*, 2006, **106**, 1375–1444.
- 21 F. Domine, M. Albert, T. Huthwelker, H.-W. Jacobi, A. A. Kokhanovsky, M. Lehning, G. Picard and W. R. Simpson, *Atmos. Chem. Phys.*, 2008, **8**, 171–208.
- 22 B. Kärcher and M. M. Basko, *J. Geophys. Res.*, 2004, **109**, D22204.
- 23 B. Kärcher, J. P. D. Abbatt, R. A. Cox, P. J. Popp and C. Voigt, *J. Geophys. Res.*, 2009, **114**, D13306.
- 24 V. F. McNeill, T. Loerting, F. M. Geiger, B. L. Trout and M. J. Molina, *Proc. Natl. Acad. Sci. U. S. A.*, 2006, **103**, 9422–9427.
- 25 S. G. Moussa, M. H. Kuo and V. F. McNeill, *Phys. Chem. Chem. Phys.*, 2013, **15**, 10989.
- 26 F. Orlando, A. Waldner, T. Bartels-Rausch, M. Birrer, S. Kato, M.-T. Lee, C. Proff, T. Huthwelker, A. Kleibert, J. van Bokhoven and M. Ammann, *Top. Catal.*, 2016, **59**, 591–604.
- 27 H. Bluhm, *J. Electron Spectrosc. Relat. Phenom.*, 2010, **177**, 71–84.
- 28 N. Ottosson, M. Faubel, S. E. Bradforth, P. Jungwirth and B. Winter, *J. Electron Spectrosc. Relat. Phenom.*, 2010, **177**, 60–70.
- 29 A. Křepelová, J. Newberg, T. Huthwelker, H. Bluhm and M. Ammann, *Phys. Chem. Chem. Phys.*, 2010, **12**, 8870.
- 30 M. Lampimäki, S. Schreiber, V. Zelenay, A. Křepelová, M. Birrer, S. Axnanda, B. Mao, Z. Liu, H. Bluhm and M. Ammann, *J. Phys. Chem. C*, 2015, **119**, 7076–7085.
- 31 J. Bischoff, F. Lutz, D. Bolmont and L. Kubler, *Surf. Sci.*, 1991, **251–252**, 170–174.
- 32 G. Franceschi, A. Conti, L. Lezuo, R. Abart, F. Mittendorfer, M. Schmid and U. Diebold, *J. Chem. Phys.*, 2024, **160**, 164312.
- 33 A. Lindblad, H. Bergersen, W. Pokapanich, M. Tchapyguine, G. Öhrwall and O. Björneholm, *Phys. Chem. Chem. Phys.*, 2009, **11**, 1758.
- 34 R. Sankari, M. Ehara, H. Nakatsuji, Y. Senba, K. Hosokawa, H. Yoshida, A. De Fanis, Y. Tamenori, S. Aksela and K. Ueda, *Chem. Phys. Lett.*, 2003, **380**, 647–653.
- 35 N. L. Prisle, N. Ottosson, G. Öhrwall, J. Söderström, M. Dal Maso and O. Björneholm, *Atmos. Chem. Phys.*, 2012, **12**, 12227–12242.
- 36 T. Gallo, G. Michailoudi, J. Valerio, L. Adriano, M. Heymann, J. Schulz, R. d. R. T. Marinho, F. Callo, N. Walsh and G. Öhrwall, *J. Phys. Chem. B*, 2024, **128**, 6866–6875.
- 37 N. Ottosson, K. J. Børve, D. Spångberg, H. Bergersen, L. J. Sæthre, M. Faubel, W. Pokapanich, G. Öhrwall, O. Björneholm and B. Winter, *J. Am. Chem. Soc.*, 2011, **133**, 3120–3130.
- 38 A. Křepelová, T. Bartels-Rausch, M. A. Brown, H. Bluhm and M. Ammann, *J. Phys. Chem. A*, 2013, **117**, 401–409.
- 39 X. Kong, A. Waldner, F. Orlando, L. Artiglia, T. Huthwelker, M. Ammann and T. Bartels-Rausch, *J. Phys. Chem. Lett.*, 2017, **8**, 4757–4762.
- 40 T. Bartels-Rausch, F. Orlando, X. Kong, L. Artiglia and M. Ammann, *ACS Earth Space Chem.*, 2017, **1**, 572–579.



- 41 A. Waldner, L. Artiglia, X. Kong, F. Orlando, T. Huthwelker, M. Ammann and T. Bartels-Rausch, *Phys. Chem. Chem. Phys.*, 2018, **20**, 24408–24417.
- 42 J. Yeh and I. Lindau, *At. Data Nucl. Data Tables*, 1985, **32**, 1–155.
- 43 G. Santachiara, F. Prodi, R. Udisti and A. Prodi, *Atmos. Res.*, 1998, **47–48**, 209–217.
- 44 C. Jaccard and L. Levi, *Z. Angew. Math. Phys.*, 1961, **12**, 70–76.
- 45 L. Levi and L. Lubart, *J. Chim. Phys. Phys.-Chim. Biol.*, 1961, **58**, 863–868.
- 46 D. E. Starr, D. Pan, J. T. Newberg, M. Ammann, E. G. Wang, A. Michaelides and H. Bluhm, *Phys. Chem. Chem. Phys.*, 2011, **13**, 19988.
- 47 J. T. Newberg and H. Bluhm, *Phys. Chem. Chem. Phys.*, 2015, **17**, 23554–23558.

